View metadata, citation and similar papers at core.ac.uk
brought to you by CORE
provided by Apollo

The Parameter Space of Atomic Layer Deposition of Ultra-Thin Oxides on Graphene

Adrianus I. Aria[†], *Kenichi Nakanishi*[†], *Long Xiao*[†], *Philipp Braeuninger-Weimer*[†], *Abhay A. Sagade*[†], *Jack A. Alexander-Webber*[†], *and Stephan Hofmann*[†*]

† Division of Electrical Engineering, Department of Engineering, University of Cambridge, United Kingdom CB3 0FA

KEYWORDS: Graphene, Atomic Layer Deposition, Aluminum Oxide, Ultra-Thin Films, Conformal Deposition

ABSTRACT

Atomic layer deposition (ALD) of ultra-thin aluminum oxide (AlO_x) films was systematically studied on supported CVD graphene. We show that by extending the precursor residence time, using either a multiple-pulse sequence or a soaking period, an ultra-thin continuous AlO_x films can be achieved directly on graphene using standard H_2O and trimethylaluminum (TMA) precursors even at a high deposition temperatures of 200°C, without the use of surfactants or other additional graphene surface modifications. To obtain conformal nucleation a precursor residence time of >2s is needed, which is not prohibitively long but sufficient to account for the slow adsorption kinetics of the graphene surface. In contrast, a shorter residence time results in heterogeneous nucleation that is preferential to defect/selective sites on the graphene. These

findings demonstrate that a careful control of the ALD parameter space is imperative in governing the nucleation behavior of AlO_x on CVD graphene. We consider our results to have model system character for rational 2D/non-2D material process integration, relevant also to the interfacing and device integration of the many other emerging 2D materials.

INTRODUCTION

Two-dimensional (2D) materials, such as graphene, offer new and improved functionalities for a wide range of applications ranging from electronics and photonics to energy conversion and storage devices.[1] The effective properties of 2D materials are, however, extremely dependent on their environment, and hence their route to applications critically requires a precise control of interfacing and integration in particular with established non-2D materials including metals, metal-oxides, and polymers. Characteristics for 2D materials are their strong, predominantly covalent, intra-layer bonding, contrasted by their weak out-of-plane interactions dominated by van der Waals forces. Due to these weak out-of-plane interactions, it remains extremely challenging to grow ultrathin continuous layers of such standard materials on top of 2D materials, be it as dielectric, barrier, dopant, contact, light emitter/absorber, carrier recombinator/separator, catalyst, or structural support.[2–10] The properties of a 2D material interfaced with a conventional thin film are thereby not merely dictated by the quality of the components. A significant challenge is to provide an optimum interface between the 2D and 3D structure, which requires a detailed understanding of the various growth modes and of 2D/non-2D material interfacing. Almost all 2D-based electrical devices, for instance, require not only metallic contacts but also interfacing to a common dielectric. While progress has been made in scalable process integration of chemical vapor deposition (CVD) of 2D materials with atomic

layer deposition (ALD) of ultra-thin metal-oxides,[7,11,12] a fundamental understanding of such interfacing remains in its infancy, hindering rational process and device design for 2D/non-2D integration.

Here, we focus on the nucleation behavior of ALD aluminum oxide (AlO_x) on supported CVD graphene, systematically exploring the ALD growth modes and the governing conditions for achieving either selective or conformal AlO_x deposition on graphene that is supported either by its original growth catalyst or transferred with various levels of defects, wrinkles and contamination. To date, the most common approaches to enhance wetting for graphene and hence to achieve a high AlO_x nucleation density and more conformal coverage employ either lower deposition temperatures (T_{dep}) or a surface modification of the graphene using seed layers, functional groups, and a more reactive oxidant to uniformly activate the graphene surface.[2,12–20] However, such approaches can not only degrade the AlO_x film properties and/or the graphene, but also introduce additional elements/states at the interface which can be deleterious to the device functionality. Hence here we do not employ any additional graphene surface modification, but rather focus on the details of the ALD parameter space. As ALD depends heavily on surface saturation to achieve the self-limiting sequential reactions, the nucleation behavior is mainly governed by three parameters: the available amount of oxidant/precursor for reaction, their mass transport to the surface, and the surface reaction kinetics.[21,22] We address the choice of these parameters in detail to control the AlO_x deposition on CVD graphene. We show that by extending the precursor residence time, by either optimizing the pulse sequences or introducing a soaking period, we are able to overcome the otherwise heterogeneous nucleation that is limited to defect/selective sites and highly dependent on support such as layer numbers and the underlying metal. As demonstrated herein, sub-2nm thin continuous AlO_x films can be

achieved directly on graphene using standard H_2O and trimethylaluminum (TMA) precursors even at a high T_{dep} of 200°C. Such a capability to directly integrate a thin continuous AlO_x film, an archetypical high-k dielectric, with graphene would allow further development of high frequency graphene FETs, for instance, as the thinning of the gate dielectric below equivalent oxide thickness (EOT) of 1 nm is highly desirable to obtain a strong current saturation while boosting transconductance (gm) and voltage gain.[23]

MATERIALS AND METHODS

AlO_x films were deposited directly by ALD on four different set of samples: graphene grown on Cu metal catalysts (G/Cu), graphene grown on Ge substrates (G/Ge), graphene transferred on SiO_2 substrates (G/SiO_2), and highly oriented pyrolytic graphite (HOPG, Agar Scientific 3.5±1.5 mosaic spread). These samples were selected to represent different types of supported graphene as it has been previously shown that AlO_x nucleation behavior is strongly affected by the underlying support.[17] The G/Cu samples were grown by CVD using H_2 diluted CH_4 (0.1% in Ar) precursor at a partial pressure of ~10^{-3} mbar and a temperature of 950–1000°C on polycrystalline Cu foils (Alfa Aesar, 25 μm thick, 99.8% purity), which have been electrochemically polished prior to the CVD using diluted H_3PO_4 (85% aqueous solution, further diluted in H_2O with 7:3 ratio) under a constant voltage of 2.7V for 7–15min.[24] The G/Ge samples were grown by CVD on monocrystalline Ge wafer (110) using H_2 diluted CH_4 (CH_4:H_2 ratio of 1:52) precursor at a partial pressure of ~1 mbar and a temperature of 920°C. The G/SiO_2 samples were fabricated by transferring the graphene layer from G/Cu onto SiO_2 substrates (Si wafer with 300nm native oxide) using polymer support (Microchem 950PMMA A4) and wet chemical etching (0.5M FeCl3 and 37% HCl), followed by a cleaning process in acetone and H_2 annealing at a partial pressure of ~1 mbar and a temperature of 200°C as described in detail elsewhere.[25,26] All CVD

and transferred graphene samples used herein were predominantly monolayer graphene with complete coverage over the substrates with size of >1x1cm^2. To ensure that the findings in this study were consistent and not skewed by changes in sample wettability due to adventitious carbon contamination from the ambient air,[24] the ALD was performed within 7 days after CVD or transfer process for G/Cu, G/Ge, and G/SiO_2, and within 15 minutes subsequent to mechanical cleaving for HOPG.

AlO_x films were deposited on all samples by ALD (Cambridge Nanotech Savannah S100 G1) using Trimethylaluminum (TMA, purity >98%, Strem Chemicals 93-1360) as the precursor and, unless stated otherwise, the vapor of deionized water (H_2O) as the oxidant that were delivered alternatingly into the reaction chamber by 20sccm of N_2 flow. During the ALD, the TMA and H_2O were volatized at temperature of 40°C, and when ozone (O_3) was used as the oxidant replacing H_2O, it was supplied by an ozone generator (DELOzone LG-7, ~90% power output) at room temperature. The deposition temperature (T_{dep}) was varied between 80–200°C. All samples were loaded and unloaded while the chamber is at T_{dep} without bringing the temperature down to room temperature. Prior to the ALD, the chamber was pumped until it reached a base pressure (P_{base}) of ~4.5x10^{-1} Torr while being purged with 20sccm of N_2 flow for at least 10min (t_{purin}). To prevent premature or CVD-like reactions, the chamber was purged after each delivery of oxidant/precursor with 20sccm of N_2 flow and purging time (t_{pur}) that varied depending on the T_{dep}: 60s purge for 80°C, 45s purge for 120°C, 30s purge for 150°C, 20s purge for 180°C, and 12s purge for 200°C. Unless stated otherwise, the total number of ALD cycle is always limited to only 12 cycles to highlight the nucleation process as a higher number of cycles usually results in a more uniform deposition. For consistency, the oxidant/precursor dose is always approximated by the product of delivery pressure (P_{dos}) and residence time (t_{dos}), which are determined by the

maximum and full-width-half-maximum (FWHM) values of the chamber pressure profile when the dose is delivered. We avoid the use of pulse time (t_{pul}) as a measurement metric as the same t_{pul} may result in different P_{dos} and t_{dos} if the carrier gas flow rate, pumping speed, and the amount of oxidant/precursor available for volatilization are varied.

To elucidate the effect of ALD parameters on the AlO_x nucleation behavior on graphene, the ALD was performed under four distinct processes: Continuous-flow Mode (CM), Pretreatment Mode (PM), Multi-pulse Mode (MM), and Stop-flow Mode (SM). Schematic representations of these processes are shown in Figure 1. CM (Fig 1a) is an ALD mode commonly used in previous literature,[12–14,18] where H_2O and TMA are dosed alternatingly into the reaction chamber and separated by the purging periods. The effect of oxidant/precursor doses was investigated by varying H_2O/TMA doses between ~0.14–~2.1Torr·s, obtained by pulsing H_2O (t_{pulA}) between 15–300ms and TMA (t_{pulB}) between 15–100ms. In CM, the doses for both H_2O and TMA are always set equally, while the dose for O_3, when it is used as the oxidant, is always set at a constant value of ~30Torr·s. PM (Fig 1b) was used here to introduce a surface modification to the sample without adding seed layers, but rather by exposure to a series of H_2O or O_3 pulses for a certain period of pretreatment time ($t_{pretreat}$) prior to AlO_x deposition. Here, $t_{pretreat}$ is varied between 10–300min for H_2O and 2–15min for O_3 pretreatments. The oxidant dose and purging time in the pretreatment period are the same as those in the subsequent deposition period, which is performed under the same conditions as in CM. The extended oxidant/precursor residence time is introduced herein by the use of a sequence of multiple pulses in MM and soaking period in SM. In MM (Fig 1c), each reactant/precursor dose is delivered by a sequence of two consecutive pulses in quick succession. The time interval (t_{intv}) between these pulses is adjusted in such a way that t_{dos} becomes the sum of FWHM of both pulses. In SM (Fig 1d), the oxidant/precursor soak

period is introduced by stopping the flow to create a static atmosphere in the process chamber for several seconds (t_{hold}) right after the oxidant/precursor is dosed. Therefore, the dose in SM is controlled by two independent parameters, t_{pul} and t_{hold}. Before the subsequent dose, the flow is continued and the chamber is purged. The effect of oxidant/precursor residence time in MM and SM was investigated by varying H_2O/TMA t_{dos} between ~2.5—~3.5s while maintaining all other ALD conditions the same as those in CM. Further details of the ALD parameters are described in the Supporting Information (section SI1).

The AlO_x nucleation was characterized by scanning electron microscopy (SEM, Carl Zeiss SIGMA VP) at acceleration voltage of 2kV and atomic force microscopy (AFM, Digital Instruments Dimension 3100) under tapping mode at a scanning frequency of 1Hz. AlO_x surface coverage (θ) was calculated based on the contrast observed in SEM images, with bright regions indicate areas of the graphene surface that are covered by AlO_x films/clusters and dark regions indicate the absence of AlO_x. Further details of the surface coverage calculation are described in the Supporting Information (section SI2).

RESULTS

Figure 2 shows the typical surface topography of CVD graphene on G/Cu prior and subsequent to ALD AlO_x using CM (Fig. 1a). Due to the nature of the CVD method used for the growth, the surface topography of G/Cu is dominated by uniaxial graphene wrinkles with an average height of 10–15nm and interspacing of 200–600nm,[27–30] which is equivalent to an average feature aspect ratio of much less than unity and an RMS surface roughness of ~5nm (Fig 2a). When the ALD is performed in CM (Fig 1a) under typical conditions of T_{dep} of 200°C and TMA/ H_2O dose of ~0.14Torr·s, which is obtained by the commonly used t_{pulA} and t_{pulB} settings of 15–

30ms,[17,31,32] the nucleation behavior on G/Cu is highly influenced by the presence of graphene wrinkles. For a low number of ALD cycles, in this case 12 cycles, AlO_x is observed to nucleate preferentially on the ridges of these wrinkles, while the troughs are still relatively, although not entirely, free from AlO_x (Fig 2b).[32] Under these ALD conditions, AlO_x deposition in the troughs occurs subsequently when the G/Cu is subjected to further ALD cycles and a high number of ALD cycles will eventually lead to a complete coverage of the G/Cu surface. This behavior was observed after 100 ALD cycles, at which point the AlO_x layer almost completely encapsulates the G/Cu surface, including in the troughs (Fig 2c). Note that the topography of the deposited AlO_x layer resembles island-like clusters, rather than a smooth film, implying a Volmer-Weber type nucleation mode.[33]

The highly selective AlO_x nucleation behavior on G/Cu at T_{dep} of 200°C leads to the assumption that a lower T_{dep} is a necessary condition for achieving a more homogeneous nucleation with H_2O/TMA.[16,17,33–35] Indeed, a significant change in AlO_x nucleation behavior could be achieved by simply altering T_{dep} while keeping the other deposition parameters constant. As shown in Figure 3a, a significantly higher nucleation density in the troughs is observed when T_{dep} is decreased to 150°C while maintaining a constant TMA/H_2O dose of ~0.14Torr·s. When T_{dep} is lowered further to 80°C, AlO_x nucleation becomes completely non-preferential, nucleating almost everywhere on the G/Cu surface yielding a surface coverage (θ) of ~98%. Note that the non-preferential nucleation is not due to the effect of insufficient purging as a too short t_{pur} will result in premature hydrolysis of TMA that impede AlO_x nucleation on graphene (see also Supporting Information section SI3). Instead, the very smooth surface topography of the AlO_x covered graphene with an RMS surface roughness of <1nm and barely visible graphene wrinkles indicates that the troughs are covered by the AlO_x more than the

ridges. This strongly suggests the occurrence of H_2O/TMA condensation when the ALD is performed at 80°C. The use of noncondensing O_3 replacing H_2O as the oxidant at T_{dep} of 80°C is shown in Figure 3b. In contrast to the nucleation obtained using H_2O at T_{dep} of 80°C, that using O_3 yields a moderately preferential nucleation on the ridges with θ of ~65%. The correlation between θ and T_{dep} in CM is shown in Figure 3d. In general, a relatively constant θ at an average value of 79-82% can be achieved in CM with a T_{dep} of 120-180°C using H_2O/TMA. A condensing condition occurs at T_{dep} of 80°C resulting in an almost complete coverage of AlO_x. On the other side of the spectrum, T_{dep} of 200°C is always observed to yield the lowest AlO_x coverage with θ ~43%, although PM (Fig 1b) can be employed to improve θ as discussed below.

The fact that CM at T_{dep} of 200°C yields the lowest AlO_x coverage gives rise to the assumption that the graphene surface needs to be uniformly activated by surface modification to obtain a more homogeneous nucleation if H_2O/TMA combination is to be used at a high T_{dep}.[2,12,13,16,18] Since the use of an additional seed layer is undesirable due to its potential deleterious effect to the device functionality, the surface modification is introduced in this study by the use of PM (Fig 1b), which is essentially an exposure to a series of H_2O or O_3 pulses for a certain period of pretreatment time ($t_{pretreat}$) followed immediately by AlO_x deposition that is similar to CM without breaking the vacuum. Aside the additional pretreatment step, the deposition parameters in PM are set to be the same as in the aforementioned CM, i.e. using a TMA/H_2O dose of ~0.14Torr·s at T_{dep} of 200°C. Figure 3c shows that a substantial shift in the AlO_x nucleation behavior is observed when $t_{pretreat}$ is set at 60min, with the nucleation is no longer preferential to the graphene ridges, but rather distributed evenly between both ridges and troughs. The change in nucleation behavior is more pronounced when $t_{pretreat}$ is prolonged further to 300min, at which point the nucleation is significantly more homogeneous throughout the G/Cu surface. Similarly,

the switch from CM to PM when O_3 is used as the oxidant not only results in a significant improvement to the nucleation density, but also completely changes the nucleation behavior as shown in Figure 3d. With $t_{pretreat}$ of just 2min, the nucleation becomes completely non-preferential and a highly conformal AlO_x layer is observed throughout the G/Cu surface. It is also important to note that the nucleation in the troughs is always found to be much more homogeneous than that on the ridges whenever O_3 pretreatment is used. The correlation between θ and $t_{pretreat}$ in PM is shown in Figure 3f. In general, the use of PM improves the AlO_x coverage on G/Cu, where θ increases proportionally with the increase of $t_{pretreat}$. While the improvement is observed regardless of whether H_2O vapor or O_3 is used as the oxidant, the effect is much more pronounced for the latter for a short $t_{pretreat}$. Using O_3/TMA, a significant improvement in θ to ~96% can be observed for $t_{pretreat}$ of just 2min, although a further increase of $t_{pretreat}$ to 15min only increases θ slightly to ~97%. In contrast, using H_2O/TMA, a significant improvement in θ to ~89% can only be observed when $t_{pretreat}$ is set to 300min. Since all deposition parameters in PM are exactly the same as in CM, the observed changes in the otherwise preferential AlO_x nucleation can all be attributed to the addition of the pretreatment step.

Previous literature has already highlighted that ALD AlO_x nucleation on monolayer graphene (MLG) can be highly dependent on the underlying graphene support/substrate.[17] Here we observe that for few-layer graphene it is also dependent on the number of graphene layers. As shown in Figures 3d and 3f, the nucleation density in the troughs of MLG is considerably higher than that in the troughs of bilayer graphene (BLG). While the use of PM, either with H_2O or O_3, results in a more homogeneous AlO_x nucleation on MLG, the nucleation on BLG is still highly selective. When PM is performed using H_2O with $t_{pretreat}$ of 60min, AlO_x shows very poor nucleation in the troughs of BLG, resulting in an extremely low θ of ~33%, approximately half

of that on MLG (Fig 3f). A significant improvement to the AlO_x nucleation on BLG can be achieved by extending the $t_{pretreat}$ to 300min. This results not only in the increase of θ on BLG to ~79% (Fig 3f), but also in the shift of the AlO_x nucleation behavior into a more homogeneous nucleation on both ridges and troughs. While a higher θ can be in general achieved using O_3 with $t_{pretreat}$ of 2min, the AlO_x nucleation density in the troughs of BLG is still much lower than that in the troughs of MLG. Note that the nucleation behavior on the ridges is unaffected by the number of graphene layers, as observed from the constant nucleation density on the ridges across the monolayer-bilayer graphene boundaries.

The failure of PM to achieve conformal AlO_x nucleation on G/Cu using H_2O/TMA at T_{dep} of 200°C motivates us here to investigate in more detail the limiting parameters at such a high T_{dep}. As ALD depends heavily on surface saturation to achieve the self-limiting reactions, there is a possibility that the aforementioned selective AlO_x nucleation on graphene is due to unsatisfied saturation conditions, and it is unclear in the literature if these conditions are always satisfied. Thus, we explore the use of higher H_2O/TMA doses than the commonly used dose with the aim of achieving surface saturation to obtain conformal AlO_x nucleation on graphene. The improvement in nucleation density under CM at a T_{dep} of 200°C due to the use of higher H_2O/TMA doses is shown in Figure 4a. While increasing the H_2O/TMA dose from ~0.14 Torr·s to ~0.3 Torr·s and ~0.56 Torr·s substantially increases the nucleation density in the troughs, the nucleation behavior itself is relatively unaltered, i.e. is still highly preferential to the ridges, suggesting that the nucleation behavior cannot be easily altered by exclusively changing the H_2O /TMA dose. Note that the AlO_x nucleation on the troughs at such a higher dose always results in a crisscrossed pattern. A transition in the nucleation behavior toward non-preferential nucleation can be observed once the H_2O/TMA dose is increased further to ~1.31 Torr·s, and consequently

an even higher H_2O/TMA dose of ~2.1 Torr·s results in a conformal nucleation of AlO_x. This finding suggest that conformal nucleation on graphene at high T_{dep} is attainable if the H_2O/TMA dose is sufficient to achieve surface saturation.

Given that the oxidant/precursor dose is essentially the product of delivery pressure (P_{dos}) and residence time (t_{dos}), a sufficiently high dose for conformal nucleation can be obtained by a higher P_{dos} and/or a longer t_{dos}. As it is not trivial to explore the effect of each parameter in CM due to the interdependency of P_{dos} and t_{dos}, i.e. both are controlled by a single parameter oxidant/precursor pulse time (t_{pul}), we introduce modifications to the ALD process, denoted herein as MM and SM, which allow us to decouple t_{dos} from P_{dos}. In MM (Fig 1c), each H_2O/TMA dose is delivered by a sequence of two consecutive pulses in quick succession such that t_{dos} is now controlled by the interval time between pulses (t_{interv}) rather than by t_{pul}. Thus, MM allows t_{dos} to be extended to about twice as long of that in the CM without changing P_{dos}. In SM (Fig 1d), the sample is soaked in H_2O/TMA dose for several seconds (t_{hold}) before being purged, allowing t_{dos} to be controlled by t_{hold} rather than by t_{pul}. Thus, SM allows t_{dos} to be completely independent from P_{dos} and extended virtually indefinitely. The use of MM and SM ALD to obtain a conformal AlO_x nucleation on G/Cu at T_{dep} of 200°C is shown in Figures 4b and 4c. A completely non-preferential nucleation can be easily obtained with a H_2O/TMA dose of ~1.12 Torr·s and a further increase in H_2O/TMA dose to ~1.65 Torr·s results in a highly homogeneous AlO_x nucleation with a complete surface coverage. Similarly, a highly homogeneous nucleation can be achieved by performing the ALD in SM with H_2O/TMA dose of just ~0.7 Torr·s. The similarity in surface topography between AlO_x deposited under SM and bare G/Cu suggest that the deposition is highly conformal.

The correlation between θ and P_{dos} for CM, MM, and SM is shown in Figure 4d, while the correlation between θ and t_{dos} is shown in Figure 4e. Although the relationship between θ and P_{dos} is observed to be approximately linear for just the CM, as an increase in dose from ~0.14 Torr·s (typical dose) to ~2.1 Torr·s results in the increase of θ from ~44% to ~99%, the overall correlation becomes extremely poor once the nucleation under MM and SM is taken into account. In contrast, a strong linear correlation between θ and t_{dos} can be observed for all ALD modes as a higher t_{dos} results in a higher θ until a saturation is achieved at t_{dos} ≥~2s. It is important to note that a conformal AlO_x nucleation is obtained with just 12 ALD cycles in MM and SM with H_2O/TMA dose <1.3 Torr·s, whereas the same dose in the CM results in a nucleation behavior that is still preferential with θ of only ~82%.

Here we also explore the use of SM to achieve conformal AlO_x nucleation at T_{dep} of 200°C on highly oriented pyrolytic graphite (HOPG), as-grown CVD graphene on Ge (G/Ge), and transferred graphene on Si (G/ SiO_2). These graphitic surfaces are known to be much less wettable by H_2O than G/Cu.[17,24] Comparisons in nucleation behavior between CM and SM at the same T_{dep} on these surfaces are shown in Figures 5a–c. AlO_x nucleation on HOPG under CM at T_{dep} of 200°C and H_2O/TMA dose of ~0.3 Torr·s (P_{dos}: ~0.3 Torr, t_{dos}: ~1s) results in an incomplete surface coverage with relatively low θ of ~68%. Despite of the low θ, the nucleation on HOPG appears to be random and non-selective to only to specific sites (Fig. 5a). On the other hand, when the CM is performed on G/Ge and G/SiO_2 under the same conditions, AlO_x nucleates selectively on specific, more highly reactive locations, resulting in an extremely low θ of just ~47% (Fig. 5b) and ~38% (Fig. 5c) respectively. Although it is more spatially irregular than that on G/Cu, AlO_x nucleation on G/SiO_2 is observed to be highly selective to the randomly oriented graphene folding and defect sites (Fig. 5c). Currently, the most common transfer method used

leads to the removal of uniaxial wrinkles that occur ubiquitously on G/Cu, but at the expense of introducing new reactive sites, including folding sites, defects, and contamination, to the graphene. As a result, AlO_x appears to nucleate preferentially on these newly introduced reactive sites. Similarly, the absence of graphene wrinkles and folding sites on G/Ge suggests that the nucleation is now preferential to domain boundaries and defect sites (Fig. 5b). On the other hand, the nucleation under SM at T_{dep} of 200°C and H_2O/TMA dose of ~0.7 Torr·s (P_{dos}: ~0.2 Torr, t_{dos}: ~3.5s) is much more homogeneous across the entire surface, resulting in AlO_x coverage with θ>97% on all samples (Fig. 5a-c). Such a homogeneous nucleation allows the formation of sub-2nm thin continuous AlO_x films, as measured by AFM (see also Supporting Information section SI4), with just 12 ALD cycles. In terms of dielectric quality, these continuous AlO_x films exhibit capacitance values of 1.6μF/cm^2 and 0.7μF/cm^2 and leakage currents of lower than 1nA at 0.7V and 2.2V when the ALD is performed in SM with H_2O/TMA dose of ~0.7 Torr·s for 20 and 50 ALD cycles respectively (see also Supporting Information section SI5). The agreement between these values and those of AlOx formation on graphene found in the literature strongly suggests that the AlO_x films deposited under SM are indeed continuous and have the potential to act as efficient high-k dielectric in graphene electronics with EOT <1.3 nm.[23,36] The fact that the difference between CM and SM used here is only in t_{dos}, i.e. t_{dos} in SM is more than three times as long as that in CM, accentuates the importance of a longer t_{dos} for obtaining homogeneous AlO_x nucleation.

Figure 5d shows the effect of AlO_x film deposition on graphene analyzed by Raman spectroscopy on G/SiO_2 prior and subsequent to ALD using 532nm excitation (see also Supporting Information section SI6 for individual representative Raman spectra). The peak intensity ratio of the 2D band and G band (I_{2D}/I_G) is found at ~2.88 for as-transferred G/SiO_2,

and shifts toward a higher value of ~3.39 after AlO_x deposition (AlO_x/G/SiO_2) for both CM and SM. Note that here CM is performed using a H_2O/TMA dose of 0.3 Torr·s at T_{dep} of 80°C while SM is performed using H_2O/TMA dose of 0.7 Torr·s at T_{dep} of 200°C, and both yield an almost complete AlO_x coverage with θ>98% on G/ SiO_2. The Raman peak intensity ratio between D band and G band (I_D/I_G) is ~0.04 for the as-transferred G/SiO_2 samples, and remains the same for AlO_x/G/SiO_2 regardless of the ALD mode used. For the as-transferred G/SiO_2, the peak frequency of the 2D band (ω_{2D}) and G band (ω_G) are found at ~2679cm^{-1} and ~1588cm^{-1}, respectively, with a ω_{2D}/ω_G slope of ~0.7. When ALD is performed in CM, ω_{2D} and ω_G are found at ~2677cm^{-1} and ~1585cm^{-1}, respectively, while when the ALD is performed in SM, they are found at ~2676cm^{-1} and ~1584cm^{-1}, respectively. Note that the ω_{2D}/ω_G slope shifts to ~2.2 for AlO_x/G/SiO_2 regardless of the ALD mode used. The line width of the 2D band (Γ_{2D}) and G band (Γ_G) are found at 29.5(±5.3) cm^{-1} and 12.8(±1.5) cm^{-1}, respectively, for the as-transferred G/SiO_2, and shift toward higher values after AlO_x deposition. When the ALD is performed in CM, the Γ_{2D} and Γ_G are found to be broadened to 32.3(±6.9) cm^{-1} and 16.4(±1.8) cm^{-1}, respectively, while when the ALD is performed in SM, they are further broadened to 33.1(±7.7) cm^{-1} and 17.2(±2.1) cm^{-1}, respectively. The Γ_{2D}/Γ_G slope is ~2.2 for all G/SiO_2 samples, with or without ALD AlO_x.

DISCUSSION

Our data show that the deposition of AlO_x on G/Cu using a typical ALD process, i.e. CM at T_{dep} of 200°C and TMA/H_2O dose of ~0.14Torr·s, is strongly affected by the presence of graphene wrinkles where the ridges form preferential AlO_x nucleation sites. These ridges are the topographically highest points on the G/Cu surface, making them more readily available sites for

the adsorption of the oxidant/precursor. More importantly, the high curvature of the ridges is known to present the most active sites on supported graphene due to the high strain in the C-C bonds.[27,37,38] Similar to the nucleation on line defects and step edges, nucleation on these ridges has been long thought to be energetically preferable to release strain and ultimately relax the graphene.[34,37] The AlO_x deposition in the troughs themselves do not take place within the first few ALD cycles, but rather starts to occur several tens of cycles later once the ridges, i.e. the most reactive sites, have been fully occupied and passivated by AlO_x clusters (Fig 2).[14,34] The highly selective nucleation behavior at such a high T_{dep} has led the heretofore conclusion in the literature that conformal AlO_x nucleation on a graphitic surface using the standard H_2O/TMA precursor is notoriously difficult to achieve, and thus a lower T_{dep} or a surface modification that promotes uniform wetting may be required.[13–17,19,20,34,39]

In terms of T_{dep}, it is widely known that an ideal ALD process can only occur in a very specific T_{dep} window.[39] A higher T_{dep} provides sufficient thermal energy to drive the surface reaction to reach completion, although it may also lead to a higher desorption rate of oxidant/precursors from the G/Cu surface that results in a highly selective nucleation to only the reactive sites with lower θ. On the other hand, a lower T_{dep} often results in not only incomplete oxidant-precursor reactions,[33,35] but also the condensation of oxidant/precursors across the sample.[39] As measured by spectroscopic ellipsometry (see Supporting Information section SI7), the refractive index of AlO_x films deposited at T_{dep} of 80°C is consistently lower, albeit only slightly, than that deposited at 200°C, suggesting that a lower T_{dep} results in a lower density in the AlO_x films.[16,40–42] In addition, the lower desorption rate at lower T_{dep} corresponds to a longer ALD process time due to a longer purge time needed between pulses.[40] Our data show that in general θ increases with the decrease of T_{dep}, where T_{dep} of 120–180°C yields an average θ of 79–75% and T_{dep} of

80°C yields an almost complete coverage with θ ~98% (Fig 3a). Thus, a lower T_{dep} is definitely favorable if the goal is to alter AlO_x deposition behavior so that the deposition occurs everywhere across the G/Cu surface.[16,17] However, the fact that the resulting AlO_x layer is topographically very flat yet porous implies that the deposition is far from the ideal conformal deposition, and is instead due to H_2O condensation that takes place mostly in the troughs. The presence of H_2O condensation at 80°C can be confirmed by replacing it with O_3, as O_3 will still be gaseous and not condense at this temperature (Fig 3a). In contrast to the AlO_x nucleation using H_2O/TMA, ALD with O_3/TMA at the same T_{dep} results in a much lower nucleation density with θ of only ~76% (Fig 3c and 3d). The absence of condensation is implied by the similarity in the AlO_x nucleation behavior between O_3/TMA at a T_{dep} of 80°C and H_2O/TMA at a higher T_{dep}, i.e. preferential nucleation on the ridges. This implies that as long as the noncondensing conditions are satisfied at low T_{dep}, the AlO_x nucleation behavior on G/Cu under CM will always be selective to the most active sites, i.e. the ridges.

A modification to the graphitic surface is often introduced to make it more wettable, either by adding seed layers and functional groups, e.g. Al and PTCA,[2,13] or by using a more reactive oxidant, e.g. O_3 and NO_2.[14,15,18] We here introduce a surface modification to the G/Cu surface by performing the ALD in PM to avoid the use of an undesirable additional seed layer and without the need to use a lower T_{dep}. When PM is performed using H_2O/TMA, it has been suggested that H_2O molecules are physically adsorbed onto the graphene surface by van der Waals forces during the pretreatment, which then act as nucleation sites for the subsequent ALD process.[16,43] A higher density of nucleation sites can be in principle achieved with a longer $t_{pretreat}$ as it leads to a higher concentration of adsorbed H_2O molecules on the G/Cu surface. However, the inter-molecular attraction between the H_2O molecules may become increasingly dominant and exceed

the van der Waals forces, resulting in island-like nucleation sites (Fig 3d).[16] Our data indeed show that at T_{dep} of 200°C, θ increases significantly with the increase of $t_{pretreat}$, despite the fact that the entire process becomes prohibitively long taking about 300min of pretreatment to reach θ of ~89% (Fig 3f). An even more effective surface modification can be introduced by performing the PM using O_3. Due to its reactivity, O_3 is commonly used to modify the graphene surface, either by cleaning the graphene surface or by functionalizing it with epoxide groups,[14,15,44–46] to ultimately change the nucleation behavior into a highly homogeneous one.[14,17,47] Indeed, a relatively short $t_{pretreat}$ of 2min is sufficient to completely alter the AlO_x nucleation behavior completely non-selective (Fig. 3f). Nevertheless, the use of O_3/TMA is less desirable as O_3 is known to have a detrimental effect on graphene, especially at a high T_{dep}.[15] To minimize damage to the graphene, T_{dep} is always set at 80°C whenever O_3/TMA is used in this study. Nevertheless, even at such a low T_{dep}, the detrimental effects of O_3 to the graphene structure could still be observed (see also Supporting Information section SI8). Therefore, a prolonged O_3 pretreatment more than 2min should be avoided as not only it does not significantly improve the AlO_x nucleation density, but also damages the graphene. In addition, the imposed upper T_{dep} limit often results in a higher carbon concentration in the deposited AlO_x layer due to incomplete decomposition of the formate or other carboxylate species,[48] which ultimately leads to a lower AlO_x density (see also Supporting Information section SI7).

While the use of PM allows a much more homogeneous AlO_x nucleation to be attained on monolayer G/Cu (MLG), it struggles to achieve the same nucleation density on bilayer G/Cu (BLG). Our data show that while AlO_x nucleation on the ridges of the BLG is very similar to that on the ridges of the MLG, the nucleation density in the troughs of BLG is significantly lower than that of MLG. Interestingly, this behavior is always observed whether H_2O or O_3 is used as

the oxidant, and although our observation is limited to only MLG and BLG, it suggests that AlO_x always nucleates preferentially on the ridges regardless of the number of graphene layers. The big difference in terms of nucleation density in the troughs may originate from the difference in polarity between MLG and BLG, where a higher number of graphene layers corresponds to a lower surface polarity.[17,24,49] It is important to note that the effect of number of graphene layers is stronger when O_3 is used as the oxidant rather than when H_2O is used, although the difference between θ of MLG and BLG can be minimized by increasing $t_{pretreat}$. As shown by our data, such a difference can be minimized to <10% after 300min of pretreatment using H_2O and to <30% after 15min of pretreatment using O_3.

As in any gas adsorption processes, the ALD process is known to be limited by the total amount of oxidant/precursor available for the reaction, quantified by the delivery pressure (P_{dos}), as well as their mass transport to the surface and the surface reaction kinetics, both are quantified by the residence time (t_{dos}).[21,22] Thus we hypothesize that a conformal AlO_x deposition can be in principle obtained using H_2O/TMA at T_{dep} of 200°C by increasing the P_{dos} to compensate for a high desorption rate from the surface and/or by extending the t_{dos} to account for the mass transport onto the not-perfectly flat surface and slow adsorption kinetics of the relatively nonreactive graphitic surface. Our data indeed show that a higher H_2O/TMA dose in CM always results in a higher AlO_x nucleation density, especially on the troughs, as reflected by the increase in θ from ~44% to ~82% when the dose is increased by an order of magnitude from ~0.14Torr·s to ~1.31Torr·s (Fig 4d). Despite the significant increase in the nucleation density on the troughs due to the use of a remarkably high H_2O/TMA dose, the nucleation behavior remains largely the same, i.e. preferential nucleation on the ridges. It is also important to note that the AlO_x nucleation in the troughs at a higher dose always results in a crisscrossed pattern (Fig 4a). While

the origin of such crisscrossed pattern is still unclear, we observe that one of the crisscrossed pattern axes is always aligned to the direction of the flow but independent to the direction of graphene wrinkles. This implies that the flow plays an important role on the nucleation behavior and may strongly affect the oxidant/precursor mass transport to the G/Cu surface. While an increase in t_{pul} in CM always yields a higher dose due to simultaneous increase of both P_{dos} and t_{dos}, care must be taken as the relation between them is not linear and highly dependent on secondary ALD parameters including carrier gas flow rate and pumping speed.

The use of MM and SM allows us here to decouple t_{dos} from P_{dos} such that a prolonged t_{dos} could be achieved without necessarily increasing t_{pul}, and consequently P_{dos}. Typically, a prolonged t_{dos} is employed to obtain conformal deposition on a high aspect ratio structures, as a longer t_{dos} is required for the oxidant/precursor molecules to fully diffuse into the structures.[50] In fact, it has been estimated that the required t_{dos} would be proportional to the square of the aspect ratio.[22] Given that the aspect ratio of the G/Cu is much less than unity, we could argue that the diffusion of oxidant/precursor molecules onto the surface should not be a limiting factor. On the other hand, the long t_{dos} may indeed be needed to account for the slow adsorption kinetics due to the inertness of the graphene surface. Our data show that for the same P_{dos}, a longer t_{dos} results in a higher θ, while for the same t_{dos}, a higher P_{dos} does not necessarily result in a higher θ. In fact, when all data from CM, MM, and SM are combined, θ can only be correlated to t_{dos} but not to P_{dos}. A strong correlation between θ and t_{dos} is observed when t_{dos} is less than a critical value of ~2s, with θ varies linearly with t_{dos}, i.e. $\theta \propto t_{dos}$, instead of with the square root of t_{dos}, i.e. $\theta \propto t_{dos}^{1/2}$, suggesting that the ALD AlO_x on G/Cu is surface reaction-limited instead of diffusion limited (Fig 4e).[50] On the other hand, a saturation is reached, i.e. $\theta \approx 100\%$, when $t_{dos} \geq \sim 2s$ regardless of the ALD mode used. In addition, the use of SM using H_2O/TMA with t_{dos} of ~3.5s

allows a much more homogeneous nucleation with θ>97% to be obtained with just 12 ALD cycles on HOPG, G/Ge, and G/SiO_2 (Fig 5a-c), negating the difficulties in introducing conformal nucleation on the notoriously difficult-to-wet graphitic surfaces. It is important to note that the value of critical t_{dos} may be different from one ALD system to another. It is also worth mentioning that the supporting substrates by themselves, e.g. bare Cu or SiO_2 without graphene, are not a difficult-to-wet surface and thus homogeneous AlO_x nucleation could be consistently obtained with the typical parameters in CM (see also Supporting Information section SI9). While a conformal nucleation on these graphitic surfaces could still possibly be obtained by CM, a prohibitively high amount of H_2O/TMA would probably be required. This finding strongly suggests that t_{dos} of H_2O/TMA needed to obtain conformal nucleation at T_{dep} of 200°C on graphitic surfaces is not excessively long.[50] More importantly, this confirms our hypothesis that t_{dos} is the key parameter to account for the slow adsorption kinetics of H_2O/TMA on the relatively nonreactive graphitic surfaces, as such the use of a lower T_{dep} and the introduction of surface modification are not a necessity for conformal AlO_x nucleation.

The Raman analysis of G/SiO_2 before and after ALD AlO_x shows that the ALD process, either in CM or SM, does not introduce additional damage to the graphene structure, as reflected from their identical I_D/I_G ratios. Thus, unlike the use of O_3 as the oxidant,[15] the use of H_2O is relatively harmless for the graphene for a range of T_{dep} from 80°C to 200°C. We also show here that t_{dos} could be extended to up to 3.5s in SM without introducing detrimental effect to the graphene even at a high T_{dep} of °C. Nevertheless, care must be taken when an extremely long t_{dos} is used as TMA is highly reactive and may result in the undesirable formation of defects on graphene (see also Supporting Information section SI10).

Although nucleation on the ridges has been long thought to be energetically preferable to release the strains to ultimately relax the graphene,[34,37] the effect of AlO_x nucleation on the mechanical strain is observed to be much less pronounced compared to its effect on charge doping of the graphene. The decrease in ω_{2D} and ω_G modes toward lower wavenumbers indicates a decrease in the graphene doping level from up to ~3x10^{12}cm^{-2} to ~10^{12}cm^{-2} when AlO_x is introduced under CM at 80°C, while the mechanical strain level remains similar in magnitude between -0.1 – -0.2% (Fig 5d).[51,52] On the other hand, when AlO_x is deposited under SM at 200°C, the doping level decreases further to <10^{12}cm^{-2} and the mechanical strain level decreases slightly to between -0.05 – -0.15%, although the broadening in Γ_{2D} and Γ_G indicates that the variation in the nanometer-scale strain is actually increased (Fig 5d).[53] It has been known that the presence of hydroxyl species on SiO2 surface induces the formation of charge trap sites that contribute to the doping level and the buckling behavior of G/SiO_2. During the ALD, the concentration of hydroxyl species on SiO2 surface is strongly reduced due to induced desorption by thermal treatments.[51,54] In addition, the surface saturation by H_2O during the ALD drives the O_2/H_2O redox reaction on SiO_2 toward H^+ that results in the depletion of reactive hydroxyl and peroxide species and leads to further removal of charge trap sites.[54,55] Thus, the difference in the doping and mechanical strain level between CM and SM may actually be attributed to the difference in T_{dep}, where a higher T_{dep} leads to a higher removal rate of charge trap sites and thus results in a lower doping and strain. Note that the level of doping and mechanical strain of graphene is strongly influenced by its substrate. Thus, the changes in doping and strain levels observed here may occur differently if the graphene is supported by substrates other than SiO_2. Nevertheless, this strongly suggests that the 12 ALD cycles in SM at 200°C is a sufficient condition not only for obtaining a homogeneous AlO_x film but also for decreasing the doping

and mechanical strain level of G/SiO_2. As mentioned earlier, the ability to homogeneously deposit ultra-thin oxide films on graphene is considered critical for device integration as, for instance, it allows a strong current saturation and a significant gain in voltage and transconductance in high-frequency graphene devices.[23] While we show that a conformal deposition on graphene is possible, its use as a barrier is yet to be investigated and its quality in terms of, for instance, leakage current, capacitance, or gas permeation, remains to be thoroughly quantified. Nevertheless, future work related to ALD on graphitic surfaces should account for the residence time if a conformal nucleation is to be achieved.

CONCLUSIONS

Our results show that the ALD of AlO_x directly on graphene using the standard H_2O/TMA precursors results in nucleation behavior that can be either highly selective or completely homogeneous across the entire surface depending on the deposition conditions. When the ALD is performed in CM under a wide range of deposition temperatures, the deposition is highly preferential to the most active sites, i.e. ridges of the graphene wrinkles, as long as a noncondensing condition is satisfied. For a condensing condition, the nucleation results in a continuous yet porous AlO_x film with complete coverage of the surface. A more homogeneous AlO_x nucleation can be achieved without relying on H_2O/TMA condensation by performing the ALD in PM, which exposes the graphene surface to H_2O prior to the actual ALD process. At a typical deposition temperature of 200°C, the use of PM allows for a more homogeneous nucleation behavior, as the nucleation density in the troughs increases proportionally with the increase of pretreatment time. Nevertheless, this is not a necessary condition as the key to obtain a conformal nucleation lies in the H_2O/TMA residence time, as an extended residence time is

needed to account for the slow adsorption kinetics of the relatively inert graphene surface. Here a prolonged residence time is introduced by an optimization to the ALD pulse sequence and a soaking period, in the form of MM and SM, respectively. Regardless of the method used, be it CM, MM, or SM, when the ALD is performed at 200°C, there exists a critical residence time, below which the nucleation is selective and above which it is much more, if not completely, homogeneous across the entire graphene surface. By extending the precursor residence time, we are able to overcome the otherwise heterogeneous nucleation such that sub-2nm thin continuous AlO_x films can be achieved directly on graphene using standard H_2O/TMA precursors even at a high T_{dep} of 200°C. As these results could be generally extended to ALD of any other oxides, particularly if homogeneous deposition is required, the work presented here should be considered as a model system for rational 2D/non-2D material process integration, which is relevant to the interfacing and device integration of other emerging 2D materials, including hBN and transition metal dichalcogenides (TMD), and many other difficult-to-wet materials.

FIGURES

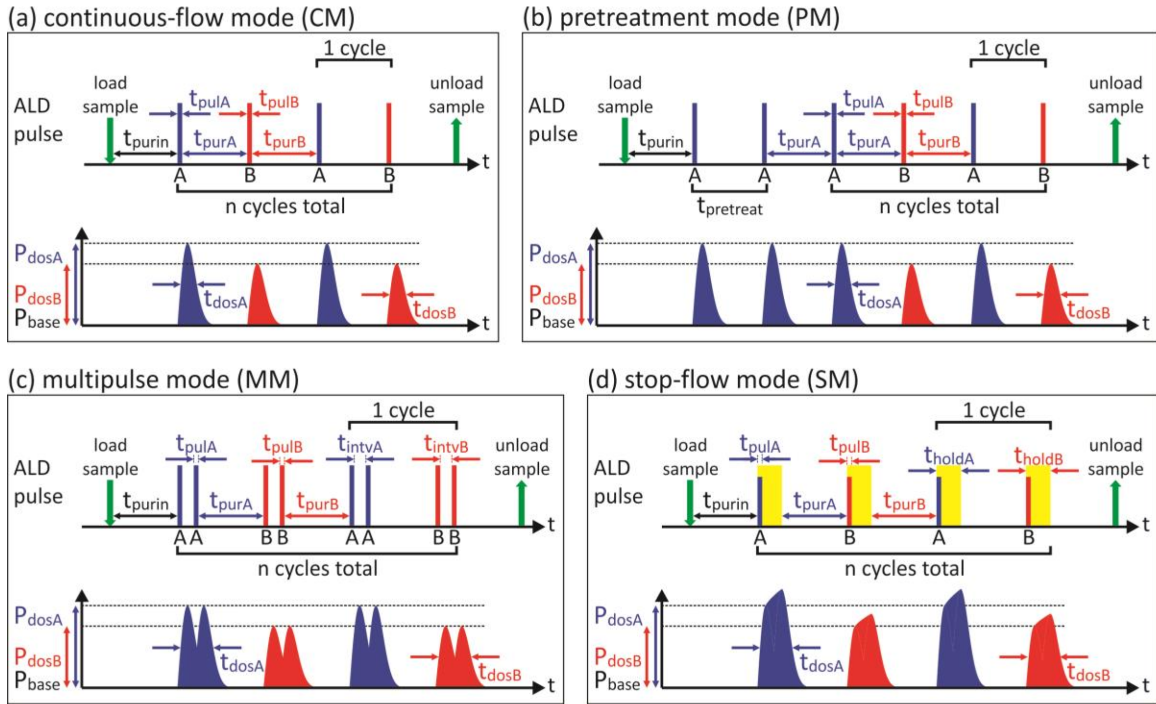

Figure 1. Schematic of the ALD process in **(a)** continuous-flow mode (CM), **(b)** pretreatment mode (PM), **(c)** multipulse mode (MM), and **(d)** stop-flow mode (SM). A denotes the oxidant, here H_2O vapor or O_3, and B denotes the metal precursor, here TMA. The oxidant/precursor dose is calculated from the product of the delivery pressure (P_{dos}) and the residence time (t_{dos}), which in CM and PM are both governed by a single parameter ALD pulse time (t_{pul}). All samples are loaded while the chamber is at the preset deposition temperature (T_{dep}) and the process chamber is purged with N_2 for more than 10min (t_{purin}) before the ALD process is started. The purge time between oxidant/precursor pulses (t_{pur}) is varied between 10s - 60s depending on T_{dep}. In PM, the samples are exposed to series of oxidant pulses prior to the ALD process, where the pretreatment time ($t_{pretreat}$) is determined by the total number of the pulses. In MM, each oxidant/precursor is delivered twice in a quick succession with a very short time interval (t_{intv}). Thus, t_{dos} in MM can be twice as long as that in CM for the same P_{dos}. In SM, the flow in the process chamber is

stopped for several seconds (t_{hold}) to allow the samples to be soaked in the oxidant/precursor. Therefore, t_{dos} in SM can be adjusted independently from P_{dos}.

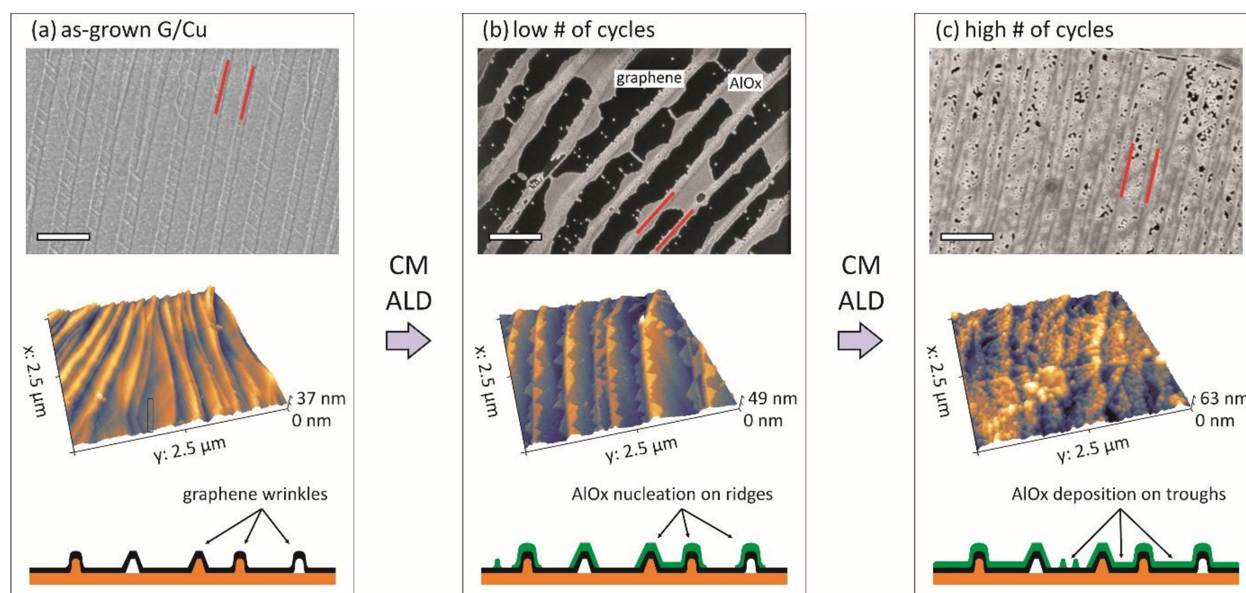

Figure 2. SEM and AFM images of typical CVD G/Cu before **(a)** and after **(b, c)** ALD of AlO_x in CM at T_{dep} of 200°C. **(a)** Surface topography of the as-grown CVD G/Cu is dominated by wrinkles with average height of 10-25nm and interspacing of 200-600nm. **(b)** AlO_x deposition on G/Cu with only 12 ALD cycles, demonstrating the nature of the nucleation process that is highly preferential to the ridges. **(c)** AlO_x deposition on G/Cu with 100 ALD cycles, demonstrating the eventual complete surface coverage due to deposition on the troughs as the number of ALD cycles increases. In **(b)** and **(c)**, the dark regions indicate uncovered graphene surface, while the bright regions indicate the presence of AlO_x clusters/films on graphene surface. All scale bars represent 500nm and the red parallel lines indicate the ridges of graphene wrinkles.

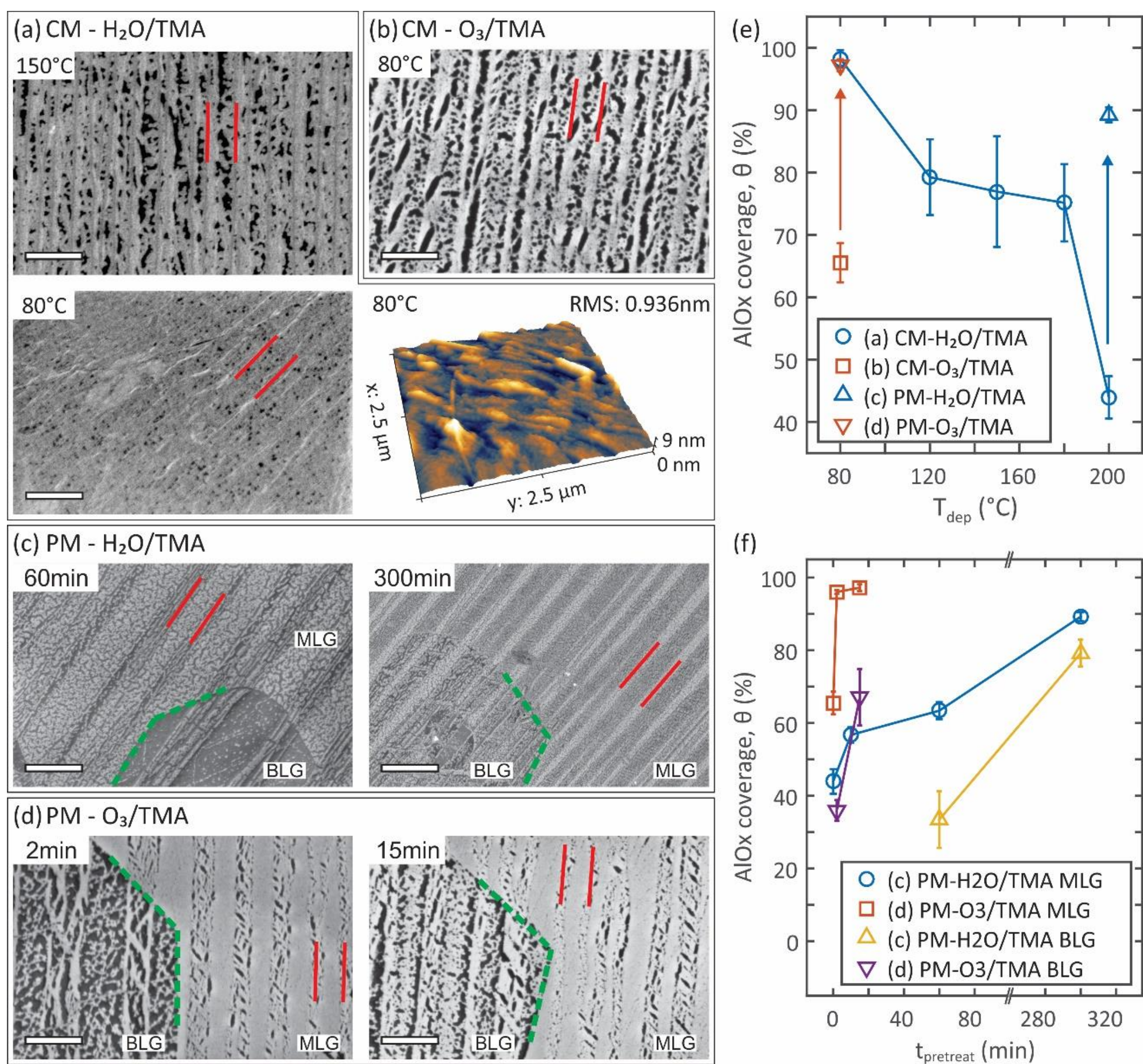

Figure 3. (a) AlO_x nucleation by ALD in CM using H_2O/TMA at T_{dep} of 150°C and 80°C. At T_{dep} of 80°C, the AlO_x coverage (θ) on G/Cu surface is almost perfectly complete with a considerably smooth surface topography, suggesting the condensation of oxidant/precursor during the ALD process. **(b)** AlO_x nucleation by ALD in CM using O3/TMA at T_{dep} of 80°C. AlO_x nucleation by ALD in PM using **(c)** H_2O/TMA with pretreatment time ($t_{pretreat}$) of 60min and 300min at Tdep of 200°C, and using **(d)** O3/TMA with $t_{pretreat}$ of 2min and 15min at T_{dep} of 80°C. The use of pretreatment significantly changes the selective nature of AlO_x nucleation into a more homogeneous nucleation. The green dotted lines in **(c)** and **(d)** indicate the boundaries

between monolayer graphene (MLG) and bilayer graphene (BLG), where the regions enclosed by the lines represent BLG. **(e)** Plot of θ on G/Cu by ALD in CM as a function of T_{dep} based on **(a)** and **(b)**. The red/blue arrows in **(e)** indicate the improvement in θ when the ALD is performed in PM, as observed in **(c)** and **(d)**, at the same T_{dep}. **(f)** Plot of θ on G/Cu surface by ALD in PM as a function of $t_{pretreat}$ as observed in **(c)** and **(d)**, where $t_{pretreat}$ of 0min corresponds to CM. All scale bars in **(a-d)** represent 500nm and the red parallel lines indicate the ridges of graphene wrinkles. Error bars in **(e)** and **(f)** indicate the standard deviation from the mean. The doses for H_2O and TMA in both CM and PM are maintained at ~0.14 Torr·s, while that for O3 is set at ~28.65 Torr·s. All AlO_x depositions are performed with 12 ALD cycles total.

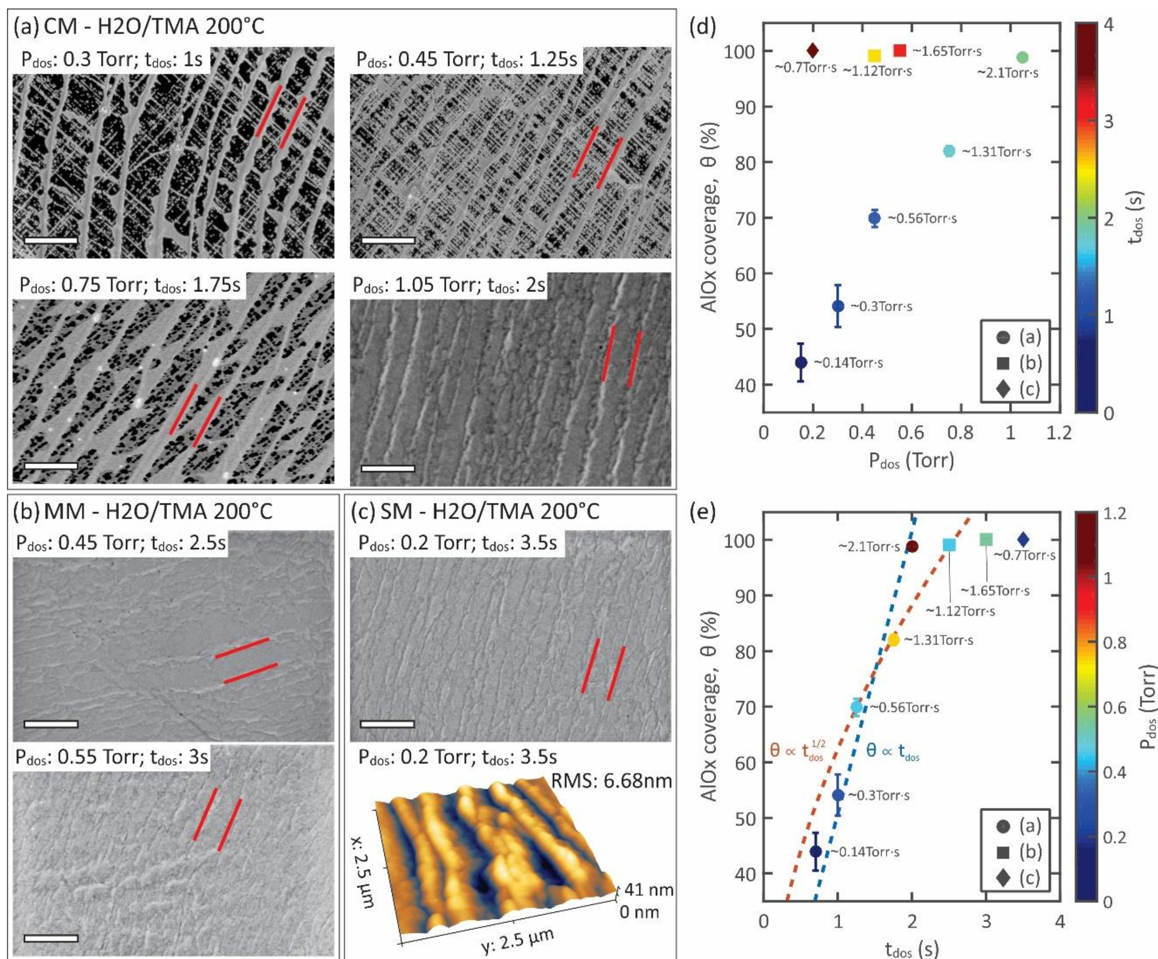

Figure 4. (a) AlO_x nucleation by ALD in CM at T_{dep} of 200°C using increasing dose of H_2O/TMA. Although the nucleation is still highly preferential to the ridges, an increase in the H_2O/TMA dose significantly improves the AlO_x nucleation especially on the troughs of G/Cu that leads to a higher θ. A full AlO_x coverage is obtained using a H_2O/TMA dose of ~2.1 Torr·s (P_{dos}: ~1.05 Torr, t_{dos}: ~2s). The typical H_2O/TMA dose as used in Figures 2 and 3 is ~0.14 Torr·s (P_{dos}: ~0.2 Torr, t_{dos}: ~0.7s). A homogeneous AlO_x nucleation on G/Cu using H_2O/TMA at T_{dep} of 200°C can also be achieved by performing the ALD either in MM **(b)** or in SM **(c)**. Under either one of these modes, H_2O/TMA residence time (t_{dos}) could be extended to reach a complete AlO_x coverage without necessarily increasing H_2O/TMA dose pressure (P_{dos}). A full AlO_x coverage can be observed in **(b)** when the H_2O/TMA dose is at ~1.65 Torr·s (P_{dos}: ~0.55Torr,

t_{dos}: ~3s) in the MM, and in **(c)** at ~0.7 Torr·s (P_{dos}: ~0.2 Torr, t_{dos}: ~3.5s) in the SM. The AlO_x surface topography in **(c)** is similar to that of as-grown G/Cu, suggesting a conformal deposition. Plot of θ on G/Cu surface by ALD in CM, MM, and SM as a function of P_{dos} **(d)** and t_{dos} **(e)**. In **(d)** the color of the marker indicates t_{dos}, while in (e) it indicates P_{dos}. In general, the relationship between θ and t_{dos} is linear, i.e. $\theta \propto t_{dos}$, instead of square root, $\theta \propto t_{dos}^{1/2}$, until a saturation is reached at $t_{dos} \geq$ ~3s. In **(a-c)**, all scale bars represent 500nm and the red parallel lines indicate the ridges of graphene wrinkles, and error bars in **(d)** and **(e)** indicate the standard deviation from the mean. All AlO_x depositions are performed with 12 ALD cycles total.

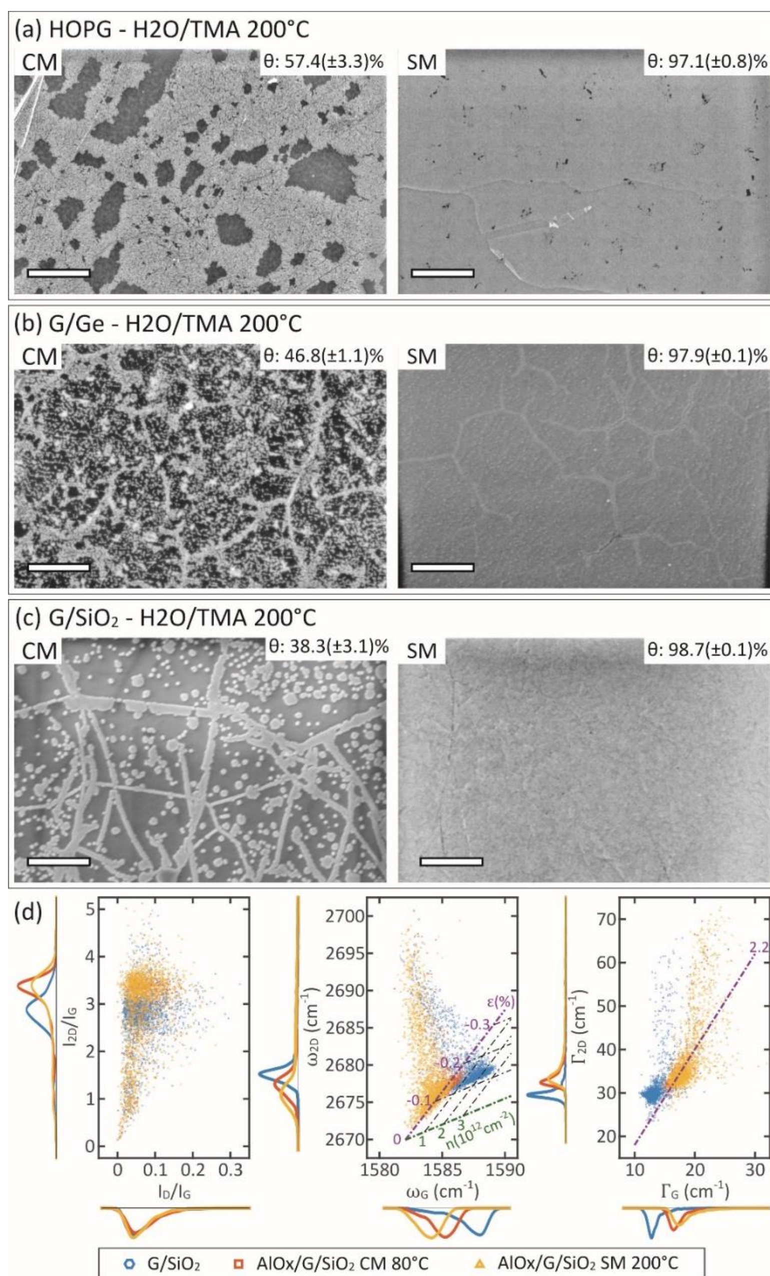

Figure 5. AlO_x nucleation on HOPG **(a)**, G/Ge **(b)**, and G/SiO_2 **(c)** by ALD in CM at T_{dep} of 200°C using H_2O/TMA dose of ~0.3 Torr·s (P_{dos}: ~0.3 Torr, t_{dos}: ~1s) for 48 cycles total and under SM at T_{dep} of 200°C using H_2O/TMA dose of ~0.8 Torr·s (P_{dos}: ~0.2 Torr, t_{dos}: ~4s) for 12 cycles total. The use of CM yields a relatively low surface coverage of ~57% on HOPG (a), ~47% on G/Ge (b), and ~38% on G/SiO_2 (c). In contrast to the nucleation behavior on HOPG

that is relatively non-preferential, that on G/Ge and G/SiO_2 is preferential to the more active locations, e.g. domain boundaries, folding sites, and contaminations introduced by the transfer process. The use of SM results in an almost perfectly conformal AlO_x nucleation with a surface coverage of >97% on all samples. All scale bars in **(a-c)** represent 500nm. **(d)** Raman spectroscopy analysis of G/SiO_2 samples before and after ALD using photon excitation of 532nm. The analysis is represented by a plot of 2D and G peak intensity ratio (I_{2D}/I_G) against D and G peak intensity ratio (I_D/I_G), a plot of 2D peak position (ω_{2D}) against G peak position (ω_G) including an indication of the relative strain and doping contributions, and a plot of 2D peak linewidth (Γ_{2D}) against G peak linewidth (Γ_G).

ASSOCIATED CONTENT

Supporting Information. Details of atomic layer deposition parameters, surface coverage calculation method, effect of purging time, thickness measurement, electronic properties measurement, ellipsometry of aluminum oxide film, nucleation on bare Cu and SiO2, and effect of prolonged ozone and TMA exposure are provided.

AUTHOR INFORMATION

Corresponding Author

* sh315@cam.ac.uk

Conflict of Interest

The authors declare no conflicts of interest.

Funding Sources

This work is supported by EPSRC (Grant No. EP/K016636/1, GRAPHTED) and ERC (Grant No. 279342, InsituNANO).

ACKNOWLEDGMENT

We acknowledge funding from EPSRC (Grant No. EP/K016636/1, GRAPHTED) and ERC (Grant No. 279342, InsituNANO). J.A.A.-W. acknowledges a Research Fellowship from Churchill College, Cambridge.

REFERENCES

(1) Ferrari, A. C.; Bonaccorso, F.; Fal'ko, V. I.; Novoselov, K. S.; Roche, S.; Bøggild, P.; Borini, S.; Koppens, F. H. L.; Palermo, V.; Pugno, N. M.; Garrido, J. a.; Sordan, R.; Bianco, A.; Ballerini, L.; Prato, M.; Lidorikis, E. E.; Kivioja, J.; Marinelli, C.; Ryhänen, T.; Morpurgo, A. F.; Coleman, J. N.; Nicolosi, V.; Colombo, L.; Fert, A.; Garcia-Hernandez, M.; Bachtold, A.; Schneider, G. F. G. F.; Guinea, F.; Dekker, C.; Barbone, M.; Sun, Z. Z.; Galiotis, C.; Grigorenko, A. N.; Konstantatos, G.; Kis, A.; Katsnelson, M. I.; Vandersypen, L. M. K.; Loiseau, A.; Morandi, V.; Neumaier, D.; Treossi, E.; Pellegrini, V.; Polini, M.; Tredicucci, A.; Williams, G. M.; Hong, B. H.; Ahn, J.-H. R. H. J.-H. H.; Kim, J. M.; Zirath, H.; van Wees, B. J.; van der Zant, H.; Occhipinti, L.; Di Matteo, A.; Kinloch, I. A.; Seyller, T.; Quesnel, E.; Feng, X. L.; Teo, K. B. K.; Rupesinghe, N. L.; Hakonen, P. J.; Neil, S. R. T.; Tannock, Q.; Löfwander, T.; Kinaret, J. M.; Hee Hong, B.; Ahn, J.-H. R. H. J.-H. H.; Min Kim, J.; Zirath, H.; van Wees, B. J.; van der Zant, H.; Occhipinti, L.; Di Matteo, A.; Kinloch, I. A.; Seyller, T.; Quesnel, E.; Feng, X. L.; Teo, K. B. K.; Rupesinghe, N. L.; Hakonen, P. J.; Neil, S. R. T.; Tannock, Q.; Löfwander, T.; Kinaret, J. M. Science and Technology Roadmap for Graphene, Related Two-Dimensional Crystals, and Hybrid Systems. *Nanoscale* **2015**, *7* (11), 4598–4810.

(2) Robinson, J. A.; Labella, M.; Trumbull, K. A.; Weng, X.; Cavelero, R.; Daniels, T.; Hughes, Z.; Hollander, M.; Fanton, M.; Snyder, D. Epitaxial Graphene Materials Integration: Effects of Dielectric Overlayers on Structural and Electronic Properties. *ACS Nano* **2010**, *4* (5), 2667–2672.

(3) Liao, L.; Bai, J.; Qu, Y.; Lin, Y.-C.; Li, Y.; Huang, Y.; Duan, X. High-κ Oxide

Nanoribbons as Gate Dielectrics for High Mobility Top-Gated Graphene Transistors. *Proc. Natl Acad. Sci. USA* **2010**, *107* (15), 6711–6715.

(4) Addou, R.; Dahal, A.; Batzill, M. Growth of a Two-Dimensional Dielectric Monolayer on Quasi-Freestanding Graphene. *Nat. Nanotechnol.* **2012**, *8* (1), 41–45.

(5) Sagade, A. A.; Neumaier, D.; Schall, D.; Otto, M.; Pesquera, A.; Centeno, A.; Elorza, A. Z.; Kurz, H. Highly Air Stable Passivation of Graphene Based Field Effect Devices. *Nanoscale* **2015**, *7* (8), 3558–3564.

(6) Yamaguchi, J.; Hayashi, K.; Sato, S.; Yokoyama, N. Passivating Chemical Vapor Deposited Graphene with Metal Oxides for Transfer and Transistor Fabrication Processes. *Appl. Phys. Lett.* **2013**, *102* (14), 143505.

(7) Martin, M.-B.; Dlubak, B.; Weatherup, R. S.; Yang, H.; Deranlot, C.; Bouzehouane, K.; Petroff, F.; Anane, A.; Hofmann, S.; Robertson, J.; Fert, A.; Seneor, P. Sub-Nanometer Atomic Layer Deposition for Spintronics in Magnetic Tunnel Junctions Based on Graphene Spin-Filtering Membranes. *ACS Nano* **2014**, *8* (8), 7890–7895.

(8) Meyer, J.; Kidambi, P. R.; Bayer, B. C.; Weijtens, C.; Kuhn, A.; Centeno, A.; Pesquera, A.; Zurutuza, A.; Robertson, J.; Hofmann, S. Metal Oxide Induced Charge Transfer Doping and Band Alignment of Graphene Electrodes for Efficient Organic Light Emitting Diodes. *Sci. Rep.* **2014**, *4*, 5380.

(9) Wang, W. S.; Wang, D. H.; Qu, W. G.; Lu, L. Q.; Xu, A. W. Large Ultrathin Anatase TiO2 Nanosheets with Exposed {001} Facets on Graphene for Enhanced Visible Light Photocatalytic Activity. *J. Phys. Chem. C* **2012**, *116* (37), 19893–19901.

(10) Liang, Y.; Li, Y.; Wang, H.; Zhou, J.; Wang, J.; Regier, T.; Dai, H. Co3O4 Nanocrystals on Graphene as a Synergistic Catalyst for Oxygen Reduction Reaction. *Nat. Mater.* **2011**, *10* (10), 780–786.

(11) Oh, I.-K.; Tanskanen, J.; Jung, H.; Kim, K.; Lee, M. J.; Lee, Z.; Lee, S.-K.; Ahn, J.-H.; Lee, C. W.; Kim, K.; Kim, H.; Lee, H.-B.-R. Nucleation and Growth of the HfO2 Dielectric Layer for Graphene-Based Devices. *Chem. Mater.* **2015**, *27* (17), 5868–5877.

(12) Shin, W. C.; Bong, J. H.; Choi, S. Y.; Cho, B. J. Functionalized Graphene as an Ultrathin Seed Layer for the Atomic Layer Deposition of Conformal High-K Dielectrics on Graphene. *ACS Appl. Mater. Interfaces* **2013**, *5* (22), 11515–11519.

(13) Wang, X.; Tabakman, S. M.; Dai, H. Atomic Layer Deposition of Metal Oxides on Pristine and Functionalized Graphene. *J. Am. Chem. Soc.* **2008**, *130* (26), 8152–8153.

(14) Lee, B.; Park, S.-Y.; Kim, H.-C.; Cho, K.; Vogel, E. M.; Kim, M. J.; Wallace, R. M.; Kim, J. Conformal Al2O3 Dielectric Layer Deposited by Atomic Layer Deposition for Graphene-Based Nanoelectronics. *Appl. Phys. Lett.* **2008**, *92* (20), 203102.

(15) Lee, B.; Mordi, G.; Kim, M. J.; Chabal, Y. J.; Vogel, E. M.; Wallace, R. M.; Cho, K. J.; Colombo, L.; Kim, J. Characteristics of High-K Al2O3 Dielectric Using Ozone-Based Atomic Layer Deposition for Dual-Gated Graphene Devices. *Appl. Phys. Lett.* **2010**, *97* (4), 43107.

(16) Zheng, L.; Cheng, X.; Cao, D.; Wang, G.; Wang, Z.; Xu, D.; Xia, C.; Shen, L.; Yu, Y.; Shen, D. Improvement of Al2O3 Films on Graphene Grown by Atomic Layer Deposition with Pre-H2O Treatment. *ACS Appl. Mater. Interfaces* **2014**, *6* (10), 7014–7019.

(17) Dlubak, B.; Kidambi, P. R.; Weatherup, R. S.; Hofmann, S.; Robertson, J. Substrate-Assisted Nucleation of Ultra-Thin Dielectric Layers on Graphene by Atomic Layer Deposition. *Appl. Phys. Lett.* **2012**, *100* (17), 173113.

(18) Young, M. J.; Musgrave, C. B.; George, S. M. Growth and Characterization of Al2O3 Atomic Layer Deposition Films on sp(2)-Graphitic Carbon Substrates Using NO2/Trimethylaluminum Pretreatment. *ACS Appl. Mater. Interfaces* **2015**, *7* (22), 12030–12037.

(19) Zhang, Y.; Qiu, Z.; Cheng, X.; Xie, H.; Wang, H.; Xie, X.; Yu, Y.; Liu, R. Direct Growth of High-Quality Al2O3 Dielectric on Graphene Layers by Low-Temperature H2O-Based ALD. *J. Phys. D. Appl. Phys.* **2014**, *47* (5), 55106.

(20) Jeong, S.-J.; Kim, H. W.; Heo, J.; Lee, M.-H.; Song, H. J.; Ku, J.; Lee, Y.; Cho, Y.; Jeon, W.; Suh, H.; Hwang, S.; Park, S. Physisorbed-Precursor-Assisted Atomic Layer Deposition of Reliable Ultrathin Dielectric Films on Inert Graphene Surfaces for Low-Power Electronics. *2D Mater.* **2016**, *3* (3), 35027.

(21) Reinke, M.; Kuzminykh, Y.; Hoffmann, P. Surface Reaction Kinetics of Titanium Isopropoxide and Water in Atomic Layer Deposition. *J. Phys. Chem. C* **2016**, *120* (8), 4337–4344.

(22) Gordon, R. G.; Hausmann, D.; Kim, E.; Shepard, J. A Kinetic Model for Step Coverage by Atomic Layer Deposition in Narrow Holes or Trenches. *Chem. Vap. Deposition* **2003**, *9* (2), 73–78.

(23) Han, S.-J.; Reddy, D.; Carpenter, G. D.; Franklin, A. D.; Jenkins, K. A. Current Saturation

in Submicrometer Graphene Transistors with Thin Gate Dielectric: Experiment, Simulation, and Theory. *ACS Nano* **2012**, *6* (6), 5520–5226.

(24) Aria, A. I.; Kidambi, P. R.; Weatherup, R. S.; Xiao, L.; Williams, J. A.; Hofmann, S. Time Evolution of the Wettability of Supported Graphene under Ambient Air Exposure. *J. Phys. Chem. C* **2016**, *120* (4), 2215–2224.

(25) Cabrero-Vilatela, A.; Weatherup, R. S.; Braeuninger-Weimer, P.; Caneva, S.; Hofmann, S. Towards a General Growth Model for Graphene CVD on Transition Metal Catalysts. *Nanoscale* **2016**, *8* (4), 2149–2158.

(26) Kratzer, M.; Bayer, B. C.; Kidambi, P. R.; Matković, A.; Gajić, R.; Cabrero-Vilatela, A.; Weatherup, R. S.; Hofmann, S.; Teichert, C. Effects of Polymethylmethacrylate-Transfer Residues on the Growth of Organic Semiconductor Molecules on Chemical Vapor Deposited Graphene. *Appl. Phys. Lett.* **2015**, *106* (10), 103101.

(27) Zhang, Y.; Fu, Q.; Cui, Y.; Mu, R.; Jin, L.; Bao, X. Enhanced Reactivity of Graphene Wrinkles and Their Function as Nanosized Gas Inlets for Reactions under Graphene. *Phys. Chem. Chem. Phys.* **2013**, *15* (43), 19042–19048.

(28) Deng, S.; Berry, V. Wrinkled, Rippled and Crumpled Graphene: An Overview of Formation Mechanism, Electronic Properties, and Applications. *Mater. Today* **2016**, *19* (4), 197–212.

(29) Zhu, W.; Low, T.; Perebeinos, V.; Bol, A. A.; Zhu, Y.; Yan, H.; Tersoff, J.; Avouris, P. Structure and Electronic Transport in Graphene Wrinkles. *Nano Lett.* **2012**, *12* (7), 3431–3436.

(30) Zhang, H.; Zhang, Y.; Wang, B.; Chen, Z.; Zhang, Y.; Sui, Y.; Yu, G.; Jin, Z.; Liu, X. Stripe Distributions of Graphene-Coated Cu Foils and Their Effects on the Reduction of Graphene Wrinkles. *RSC Adv.* **2015**, *5* (117), 96587–96592.

(31) Garces, N. Y.; Wheeler, V. D.; Hite, J. K.; Jernigan, G. G.; Tedesco, J. L.; Nepal, N.; Eddy, C. R.; Gaskill, D. K. Epitaxial Graphene Surface Preparation for Atomic Layer Deposition of Al2O3. *J. Appl. Phys.* **2011**, *109* (12), 124304.

(32) Van Lam, D.; Kim, S.-M.; Cho, Y.; Kim, J.-H.; Lee, H.-J.; Yang, J.-M.; Lee, S.-M. Healing Defective CVD-Graphene through Vapor Phase Treatment. *Nanoscale* **2014**, *6* (11), 5639–5644.

(33) Puurunen, R. L. Surface Chemistry of Atomic Layer Deposition: A Case Study for the Trimethylaluminum/Water Process. *J. Appl. Phys.* **2005**, *97* (12), 121301.

(34) Xuan, Y.; Wu, Y. Q.; Shen, T.; Qi, M.; Capano, M. A.; Cooper, J. A.; Ye, P. D. Atomic-Layer-Deposited Nanostructures for Graphene-Based Nanoelectronics. *Appl. Phys. Lett.* **2008**, *92* (1), 13101.

(35) Zheng, L.; Cheng, X.; Yu, Y.; Xie, Y.; Li, X.; Wang, Z. Controlled Direct Growth of Al2O3 -Doped HfO2 Films on Graphene by H2O-Based Atomic Layer Deposition. *Phys. Chem. Chem. Phys.* **2015**, *17* (5), 3179–3185.

(36) Yeh, C.-H.; Lain, Y.-W.; Chiu, Y.-C.; Liao, C.-H.; Moyano, D. R.; Hsu, S. S. H.; Chiu, P.-W. Gigahertz Flexible Graphene Transistors for Microwave Integrated Circuits. *ACS Nano* **2014**, *8* (8), 7663–7670.

(37) Kim, K.; Lee, H.-B.-R.; Johnson, R. W.; Tanskanen, J. T.; Liu, N.; Kim, M.-G.; Pang, C.;

Ahn, C.; Bent, S. F.; Bao, Z. Selective Metal Deposition at Graphene Line Defects by Atomic Layer Deposition. *Nat. Commun.* **2014**, *5*, 4781.

(38) Wu, Q.; Wu, Y.; Hao, Y.; Geng, J.; Charlton, M.; Chen, S.; Ren, Y.; Ji, H.; Li, H.; Boukhvalov, D. W.; Piner, R. D.; Bielawski, C. W.; Ruoff, R. S. Selective Surface Functionalization at Regions of High Local Curvature in Graphene. *Chem. Commun. (Cambridge, U. K.)* **2013**, *49* (7), 677–679.

(39) George, S. M. Atomic Layer Deposition: An Overview. *Chem. Rev.* **2010**, *110* (1), 111–131.

(40) Groner, M. D.; Fabreguette, F. H.; Elam, J. W.; George, S. M. Low-Temperature Al2O3 Atomic Layer Deposition. *Chem. Mater.* **2004**, *16* (4), 639–645.

(41) Saleem, M. R.; Ali, R.; Honkanen, S.; Turunen, J. Thermal Properties of Thin Al2O3 Films and Their Barrier Layer Effect on Thermo-Optic Properties of TiO2 Films Grown by Atomic Layer Deposition. *Thin Solid Films* **2013**, *542*, 257–262.

(42) Ylivaara, O. M. E.; Liu, X.; Kilpi, L.; Lyytinen, J.; Schneider, D.; Laitinen, M.; Julin, J.; Ali, S.; Sintonen, S.; Berdova, M.; Haimi, E.; Sajavaara, T.; Ronkainen, H.; Lipsanen, H.; Koskinen, J.; Hannula, S.-P.; Puurunen, R. L. Aluminum Oxide from Trimethylaluminum and Water by Atomic Layer Deposition: The Temperature Dependence of Residual Stress, Elastic Modulus, Hardness and Adhesion. *Thin Solid Films* **2014**, *552*, 124–135.

(43) Cao, Y.-Q.; Cao, Z.-Y.; Li, X.; Wu, D.; Li, A.-D. A Facile Way to Deposit Conformal Al2O3 Thin Film on Pristine Graphene by Atomic Layer Deposition. *Appl. Surf. Sci.* **2014**, *291*, 78–82.

(44) Li, Z.; Wang, Y.; Kozbial, A.; Shenoy, G.; Zhou, F.; McGinley, R.; Ireland, P.; Morganstein, B.; Kunkel, A.; Surwade, S. P.; Li, L.; Liu, H. Effect of Airborne Contaminants on the Wettability of Supported Graphene and Graphite. *Nat. Mater.* **2013**, *12* (10), 925–931.

(45) McDonnell, S.; Pirkle, A.; Kim, J.; Colombo, L.; Wallace, R. M. Trimethyl-Aluminum and Ozone Interactions with Graphite in Atomic Layer Deposition of Al2O3. *J. Appl. Phys.* **2012**, *112* (10), 104110.

(46) Aria, A. I.; Gani, A. W.; Gharib, M. Effect of Dry Oxidation on the Energy Gap and Chemical Composition of CVD Graphene on Nickel. *Appl. Surf. Sci.* **2014**, *293*, 1–11.

(47) Jandhyala, S.; Mordi, G.; Lee, B.; Lee, G.; Floresca, C.; Cha, P.-R.; Ahn, J.; Wallace, R. M.; Chabal, Y. J.; Kim, M. J.; Colombo, L.; Cho, K.; Kim, J. Atomic Layer Deposition of Dielectrics on Graphene Using Reversibly Physisorbed Ozone. *ACS Nano* **2012**, *6* (3), 2722–2730.

(48) Goldstein, D. N.; McCormick, J. A.; George, S. M. Al2O3 Atomic Layer Deposition with Trimethylaluminum and Ozone Studied by in Situ Transmission FTIR Spectroscopy and Quadrupole Mass Spectrometry. *J. Phys. Chem. C* **2008**, *112* (49), 19530–19539.

(49) Munz, M.; Giusca, C. E.; Myers-Ward, R. L.; Gaskill, D. K.; Kazakova, O. Thickness-Dependent Hydrophobicity of Epitaxial Graphene. *ACS Nano* **2015**, *9* (8), 8401–8411.

(50) Elam, J. W.; Routkevitch, D.; Mardilovich, P. P.; George, S. M. Conformal Coating on Ultrahigh-Aspect-Ratio Nanopores of Anodic Alumina by Atomic Layer Deposition. *Chem. Mater.* **2003**, *15* (18), 3507–3517.

(51) Lee, J. E.; Ahn, G.; Shim, J.; Lee, Y. S.; Ryu, S. Optical Separation of Mechanical Strain from Charge Doping in Graphene. *Nat. Commun.* **2012**, *3*, 1024.

(52) Boscá, A.; Pedrós, J.; Martínez, J.; Palacios, T.; Calle, F. Automatic Graphene Transfer System for Improved Material Quality and Efficiency. *Sci. Rep.* **2016**, *6*, 21676.

(53) Neumann, C.; Reichardt, S.; Venezuela, P.; Drögeler, M.; Banszerus, L.; Schmitz, M.; Watanabe, K.; Taniguchi, T.; Mauri, F.; Beschoten, B.; Rotkin, S. V; Stampfer, C. Raman Spectroscopy as Probe of Nanometre-Scale Strain Variations in Graphene. *Nat. Commun.* **2015**, *6*, 8429.

(54) Zheng, L.; Cheng, X.; Cao, D.; Wang, Z.; Xia, C.; Yu, Y.; Shen, D. Property Transformation of Graphene with Al2O3 Films Deposited Directly by Atomic Layer Deposition. *Appl. Phys. Lett.* **2014**, *104* (2), 23112.

(55) Levesque, P. L.; Sabri, S. S.; Aguirre, C. M.; Guillemette, J.; Siaj, M.; Desjardins, P.; Szkopek, T.; Martel, R. Probing Charge Transfer at Surfaces Using Graphene Transistors. *Nano Lett.* **2011**, *11* (1), 132–137.

Table of Contents

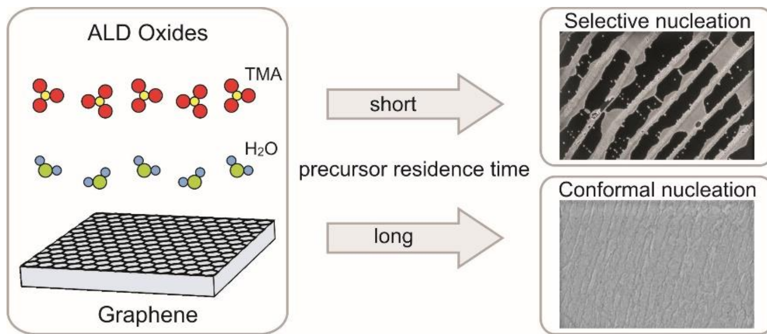
ALD Oxides
TMA
H2O
Graphene
short
precursor residence time
long
Selective nucleation
Conformal nucleation